Reliability analysis of offshore wind turbine foundations under lateral cyclic loading

Gianluca Zorzi[1], Amol Mankar[2], Joey Velarde[3], John D. Sørensen[2], Patrick Arnold[1], Fabian Kirsch[1]

[1] GuD Geotechnik und Dynamik Consult GmbH, Berlin, 10589, Germany

5 [2] Aalborg University, Aalborg, 9100, Denmark

[3] COWI A/S, Aarhus, 8000, Denmark

Correspondence to: Gianluca Zorzi (zorzi@gudconsult.de)

Abstract. The design of foundations for offshore wind turbines (OWT) requires the assessment of the long-term performance of the soil-structure-interaction (SSI) which is subjected to a large number of cyclic loadings. In terms of

10 serviceability limit state (SLS), it has to be ensured that the foundation does not exceed the operational tolerance prescribed by the wind turbine manufacturer throughout its lifetime. This work aims at developing a probabilistic approach along with a reliability framework with emphasis on verifying the SLS criteria in terms of maximum allowable rotation during an extreme cyclic loading event. This reliability framework allows the quantification of uncertainties in soil properties, in the constitutive soil model for cyclic loadings and extreme environmental conditions and verifies that the foundation design

15 meets a specific target reliability level. A 3D finite element (FE) model is used to predict the long-term response of the SSI accounting for the accumulation of permanent cyclic strain experienced by the soil. The proposed framework is employed for the design of a large diameter monopile supporting a 10 MW offshore wind turbine.

1 Introduction

Adopting the limit state design philosophy, the geotechnical design of offshore foundations is mainly governed by two limit

20 states: i.e. the ultimate limit state (ULS) and the serviceability limit state (SLS). Mostly, the design of an offshore structure starts with the ULS phase in which a loop between geotechnical and structural engineers is required to converge to a set of optimal design dimensions. The ULS design must ensure that the soil's bearing capacity withstands the lateral loading of the pile within the allowable deformations. Subsequently the SLS design (also called long-term verification) criteria is employed to verify the safety of the soil-structure-interaction (SSI) throughout the planned operational lifetime. During this lifespan,

25 OWT are subjected to a high amount of cyclic loadings (winds and waves) which can change the long-term performance of the SSI. There are two main factors influencing the SSI and thus the SLS design of an offshore wind turbine foundation subjected to long-term cyclic loading (Bhattacharya, 2014):

(1) Accumulated permanent rotation (tilting) due to the development of plastic strain in the soil.

(2) Structural stiffening or softening due to changes in soil properties.

30 Where this work focusses on the first issue. During the design phase, wind turbine manufacturers provide a tilting restriction for operational reasons. The recommended practice DNV-GL-RP-C212 (DNV-GL, 2017) gives an example of the order of magnitude for the maximum allowed tilting of 0.25° throughout the planned lifetime. This strict verticality requirement may have originated from different design criteria which however are mainly rooted within the onshore wind turbine sector (Bhattacharya, 2019):

35 - Blade-tower collision: due to an initial deflection of the blades, a possible tilting of the tower may reduce the blade-tower clearances;

- Reduced energy production: change in the attack angle (wind-blades) may reduce the total energy production;

- Yaw motors and yaw breaks: reducing motor capacity for yawing into the wind;

- Nacelle bearing: a tilted nacelle may experience different loadings in the bearing, causing a reduction of their
40   fatigue life or restrict their movements;

- Variation in fluid levels and cooling fluid movement;

- P-δ effect: the mass of the rotor-nacelle-assembly is not aligned with the vertical axis and creates an additional overturning moment in the tower, foundation, grouted connection and in the soil surrounding the foundation;

- Aesthetic reasons.

45 In SLS designs, extreme as well as relevant accidental loads, such as typhoons and earthquakes, should be accounted for since they can be design-driving loads. A very strict tilting requirement, i.e. 0.25°, in conjunction with these accidental conditions can increase the foundation dimension and significantly raise the cost of the foundation.

The long-term behaviour of the SSI is usually not accounted for directly in most projects due to the lack of universally accepted numerical and conceptual methods. To fill this gap, an advanced numerical method called soil cluster degradation
50 (SCD) method was developed (Zorzi et al., 2018). This method explicitly predicts the cyclic response of the SSI in terms of foundation rotation. The main objective of this paper is to use the SCD method within a probabilistic approach. The probabilistic approach along with the reliability framework is used to quantify the main uncertainties (aleatoric and epistemic), explore which uncertainty the response is most sensitive to and design the long-term behaviour of the foundation for a specific target reliability level. In this paper first the developed reliability-based design (RBD) framework is outlined in
55 detail. Finally an application of the proposed RBD framework is presented for a large diameter monopile supporting a 10 MW offshore wind turbine.

2 Development of the RBD framework

2.1 Limit state function for SLS

The rotation experienced by the foundation structure subjected to cyclic loading is considered partially irreversible
60 (irreversible serviceability limit states) because the soil develops an accumulation of irreversible deformation due to the

cyclic loading action. For this reason, it is noted that the accidental and environmental load cases for the SLS design are the extreme loads which give the highest rotation. As for a deterministic analysis, the first step in reliability-based analysis is to define the structural failure condition(s). The term *failure* signifies here the infringement of the serviceability limit state criteria which is here set to a tilting more than 0.25°. The limit state function $g(\boldsymbol{X})$ can then be written as

65 $$g(\boldsymbol{X}) = \theta_{max} - \theta_{calc}(\boldsymbol{X}) \,, \tag{1}$$

where $\theta_{max} = 0.25°$ is the maximum allowed rotation and $\theta_{calc}(\boldsymbol{X})$ is the predicted rotation (i.e. the model response) based on a set of input stochastic variable $\boldsymbol{X}$.

2.2 Estimation of the probability of failure

The design has to be evaluated in terms of the probability of failure. The probability of failure is defined as the probability of
70 the calculated value of rotation $\theta_{calc}(\boldsymbol{X})$ exceeding the maximum allowed rotation θ_{max} as it does when the limit state function $g(\boldsymbol{X})$ becomes negative, i.e.:

$$P_f = \mathrm{P}[g(\boldsymbol{X}) \leq 0] = P[\theta_{max} \leq \theta_{calc}(\boldsymbol{X})] \,, \tag{2}$$

Once the probability of failure is calculated, the reliability index β is estimated by taking the negative inverse standard normal distribution of the probability of failure:

75 $$\beta = \Phi^{-1}(P_f) \,, \tag{3}$$

where $\Phi(\,)$ is the standard normal distribution function. The probability of failure in this paper is estimated using Monte-Carlo (MC) simulation. For each realization, MC randomly picks a sequence of random input variables, calculate the model response $\theta_{calc}(\boldsymbol{X})$ and checks if $g(\boldsymbol{X})$ is negative (Fenton and Griffiths, 2008). Thus for a total of n realisations the probability of failure can be computed as:

80 $$P_f = \frac{n_f}{n} \,, \tag{4}$$

with n_f being the number of realizations for which the limit state function is negative (rotation higher than 0.25 °).

The IEC 61400-1 (IEC, 2009) sets as a requirement with regards to safety of wind turbine structures, a maximum annual probability of failure equal to $5 \cdot 10^{-4}$ (ULS target reliability level). Usually, in the Eurocodes the characteristic SLS limit is used for irreversible SLS. In EN1990 Annex B an annual target reliability index for SLS equal to 2.9 is indicated,
85 corresponding to an annual probability of failure equal to $2 \cdot 10^{-3}$.

The IEC61400-1 does not specify target reliability levels for SLS condition. Therefore, it can be argued that the target for SLS should be in the range of $5 \cdot 10^{-4}$ - $2 \cdot 10^{-3}$. In this paper the same reliability target for ULS of $5 \cdot 10^{-4}$ is also considered for the irreversible SLS as a conservative choice.

2.3 Derivation of the model response θ_{calc}

90   The calculation of the model response θ_{calc} is based on the soil cluster degradation (SCD) model. The SCD method explicitly predicts the long-term response of an offshore foundation accounting for the cyclic accumulation of permanent strain in the soil. The SCD model is based on 3D finite element (FE) simulations in which the effect of the cyclic accumulation of permanent strain in the soil is taken into account through the modification of a fictional elastic shear modulus in a cluster-wise division of the soil domain. Reduction of the soil modulus is based on the cyclic contour diagram

95   framework (Andersen, 2015). The loading input for the model must be a design storm event simplified in a series of regular parcels. This loading assumption is also recommended by DNV-GL-RP-C212 (DNV-GL, 2017) and the BSH standard (BSH, 2015). The method is implemented in the commercial code PLAXIS 3D (PLAXIS, 2017).

Three stochastic input variables ($X = [X_1, X_2, X_3]$) are necessary for the SCD model:

- X_1 = soil stiffness that is derived from cone penetration test (CPT)
100   - X_2 = cyclic contour diagram that is derived from cyclic laboratory tests
- X_3 = extreme environmental loads that are derived from metocean data and a fully-coupled aero-hydro-servo-elastic model.

These inputs have to be quantified in terms of their point statistics (e.g. the mean, standard deviation, probability distribution type) representing the uncertainties. Using MC simulation, $100/p_f$ realizations can be needed to estimate an accurate

105   probability of failure, which makes it challenging to apply it in combination with FE simulations. Since the SCD model is based on 3D FE simulations, it is computationally intensive and expensive to complete a large amount of realizations. One FE simulation takes approximately 30-40 minutes. For this reason, a response surface (RS) is trained in such a way that it yields the same model response θ_{calc} as the SCD model for the studied range of the input variables X. The design of experiment (DoE) procedure is used to explore the most significant combinations of the input variables X. Based on the

110   developed FE simulations plan, the obtained outputs θ_{calc} are used to fit the response function.

Figure 1 summarizes the methodology for the reliability analysis design for lateral cyclic loading. The framework starts with the uncertainty quantification from the available data (CPT, cyclic laboratory tests of the soil and metocean & aero-hydro-servo-elastic model) and the derivation of the stochastic input variables (soil stiffness, cyclic contour diagram and storm event). Based on the stochastic input variables, a response surface is then trained to yield the same output (in terms of

115   structural tilting) of the 3D FE simulations. The response surface is then used to calculate the probability of failure passing through the formulation of the limit state equation and Monte Carlo simulation. If the calculated probability of failure does

not meet the target probability, then the foundation geometry has to be changed and the methodology repeated to check whether the new design is safe.
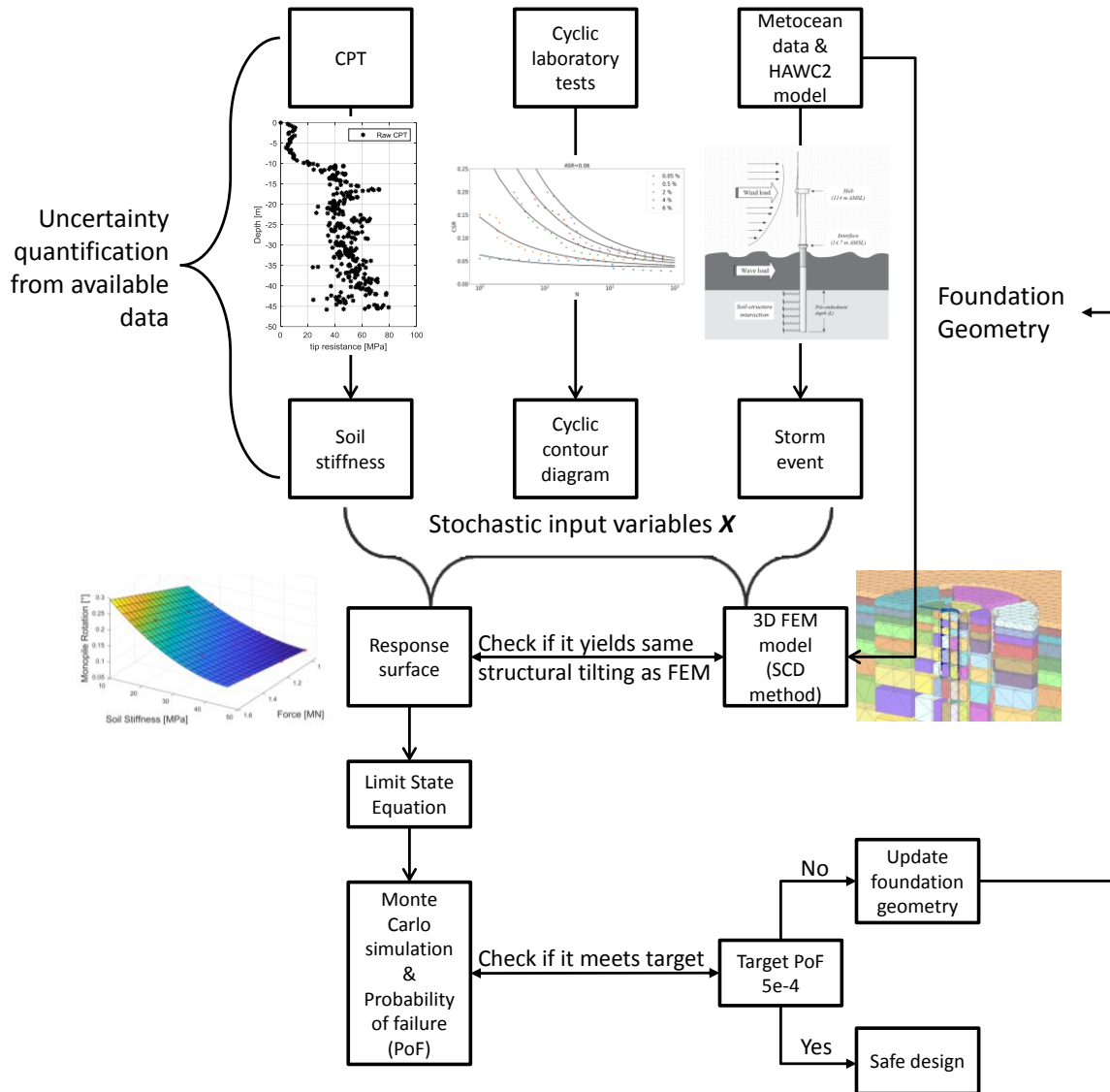
Figure 1: Methodology of reliability analysis.

3. Case study: Reliability design for a monopile supporting a 10MW wind turbine

First, this chapter goes through the subsoil conditions and the ULS design of the monopile geometry supporting a 10 MW wind turbine. Then the reliability framework shown in Figure 1 is applied to the monopile to check if the design satisfies the SLS criteria. The following chapters discuss derivation of input uncertainties for the SCD method, derivation of the response surface and probability of failure and reliability index calculation.

3.1 Monopile design: subsoil condition and pile geometry

For the present case study, a tip resistance from the cone penetration test and the boring profile are used to determine the geotechnical properties and soil stratigraphy at the site where the monopile is assumingly installed. The CPT, shown in Figure 2, features an increase of the tip resistance with increasing depth, which is typical for sand. In combination with the

130   borehole profile, the tip resistance from the CPT suggests that the soil can be divided into two different layers. At approximately -10 meter there is a jump in the tip resistance marking a transition to another layer with a higher magnitude visible, leading to the conclusion that denser sand is present. The characterization of the soil extracted from the boreholes, shows the first layer (from 0 to -10 m) consisting of fine to medium sand and the second layer (from -10 m) of well graded sand with fine gravel.
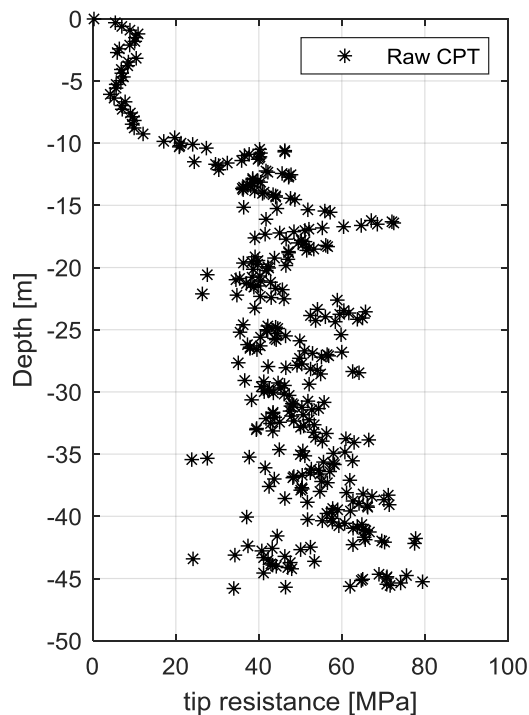
135

Figure 2: CPT profile.

In order to accurately predict the soil-structure-interaction and incorporate the rigid behaviour of large diameter monopile, the ULS geotechnical verification of the preliminary design of the monopile is carried out, using the finite element method in PLAXIS 3D.

140   The monopile in PLAXIS is modelled as a hollow steel cylinder using plate elements. For the steel, a linear elastic material is assumed with Young's modulus of 200 GPa and Poisson coefficient of 0.3. Interface elements are used to account for the reduced shear strength at the pile's surface.

The soil model used is the Hardening Soil model with small-strain stiffness (HSsmall). The soil model parameters for the two layers are derived from the tip resistance (Figure 2) and listed in Table 1. The relative density of the two layers is calculated using the formula from Baldi et al. (Baldi et al., 1986) with the over-consolidated parameters leading to a mean value of 70% and 90% for the first and second layer, respectively.

Soil	Parameter	Value	Soil	Parameter	Value
Fine-medium sand	E_{50} [MPa]	33.3	Medium-coarse sand	E_{50} [MPa]	98.3
	E_{oed} [MPa]	33.3		E_{oed} [MPa]	98.3
	E_{ur} [MPa]	99.9		E_{ur} [MPa]	295
	m [-]	0.5		m [-]	0.5
Depth: from 0 to -10 m	c [kN/m2]	0.1	Depth: from -10 m	c [kN/m2]	0.1
	φ [°]	39		φ [°]	42
	ψ [°]	9		ψ [°]	12
	G_0 [MPa]	116		G_0 [MPa]	196.6
Relative density: 70%	$\gamma_{0.7}$ [$-$]	0.0001	Relative density: 90%	$\gamma_{0.7}$ [$-$]	0.0001

Table 1: Soil model parameters.

The monopile design requires a loop between the structural and geotechnical engineers in order to update the soil stiffness and loads at the mudline level. A fully-coupled aero-hydro-servo-elastic model using HAWC2 (Larsen and Hansen, 2015) is developed to perform the time-domain wind turbine load simulations (Velarde et al., 2019b). The soil structure interaction model is based on the Winkler-type approach, which features a series of uncoupled nonlinear soil springs (so called p-y curves) distributed at every 1 m. The force (p) - deformation (y) relations are extracted from the PLAXIS 3D model. At each meter section, the calculation of the force (p) is done by integrating the stresses along the loading direction over the surface. The displacement (y) is taken as the plate's displacement.

The final pile design consists of an outer pile diameter at mudline level of 8 m, the pile thickness of 0.11 m and the pile embedment length of 29 m. The natural frequency of the monopile is 0.2 Hz and designed to be within the soft-stiff region. Fatigue analysis of the designed monopile is also carried out (Velarde et al., 2019b). Figure 3.a shows the horizontal displacement contour plot at 3.5 MN horizontal force. Figure 3.b shows the horizontal load-rotation curve at mudline.

A   b
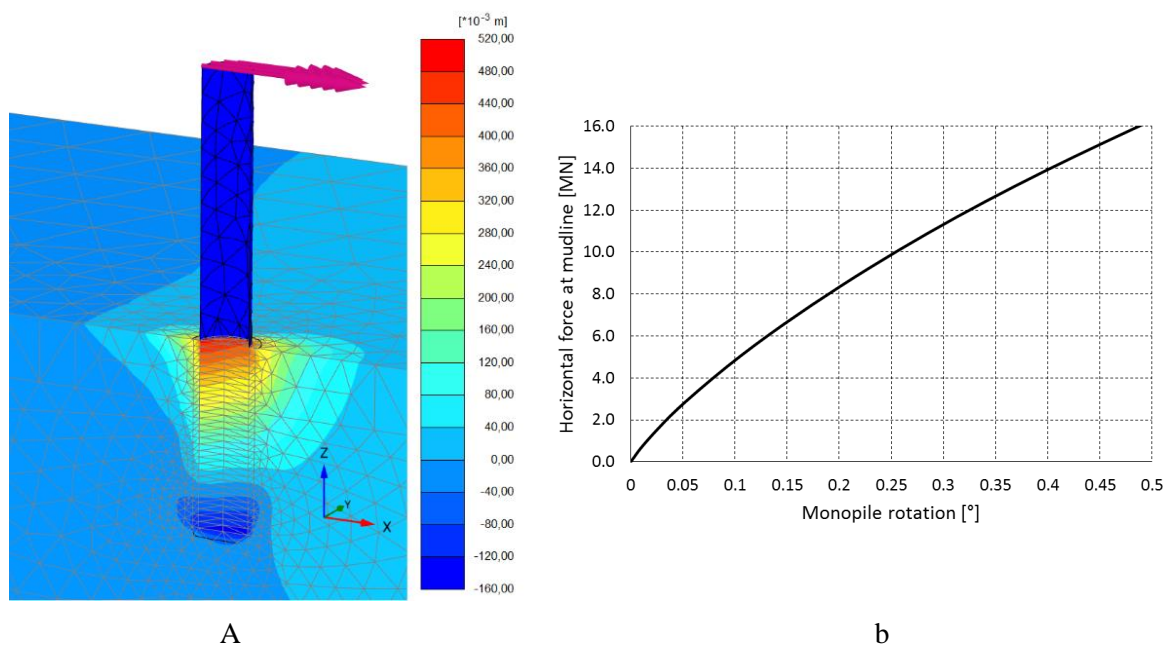
Figure 3: (a) Horizontal displacement contour plot at 3.5 MN horizontal load; (b) Monopile rotation.

3.2 Input uncertainties for the SCD model

The application of the SCD model requires three inputs: soil stiffness, cyclic contour diagrams and a design storm event. Laboratory testing and field measurements are used in order to estimate the inputs for the model. In this estimation process different sources of uncertainty of unknown magnitude are introduced (Wu et al., 1989). These parameters then have to be modelled as stochastic variables with a certain statistical distribution.

3.2.1 Soil Stiffness

The uncertainties of the soil stiffness used in the SCD model is analysed. The soil model employed in the SCD method is the Mohr-Coulomb model with a stress-depended stiffness (i.e. stiffness increases with depth). For cyclic loading problems, the unloading-reloading Young's modulus E_{ur} is used. This soil modulus is obtained from the tip resistance from the CPT test (Figure 2). The layering of the soil domain is assumed to be deterministic as explained in chapter 3.1.
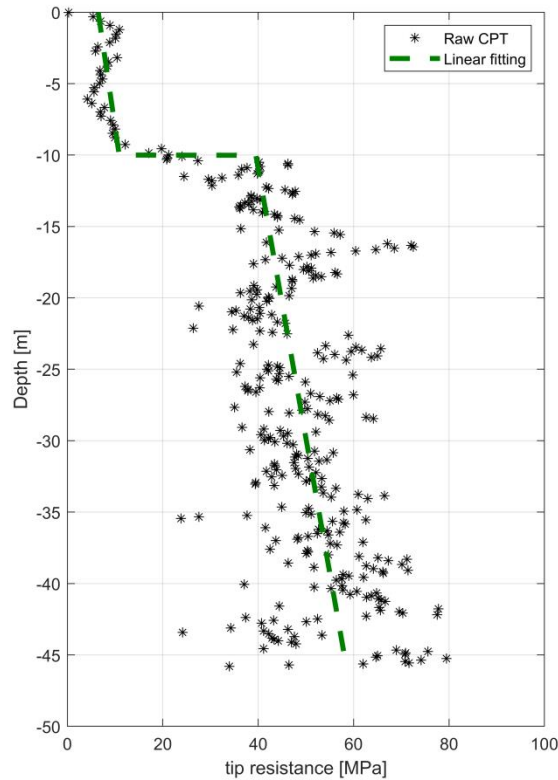
Figure 4: Average tip resistance.

The design tip resistance is established by means of the best-fit line in the data. A linear model is fitted to the data for each layer (Figure 4, green line). Maximum likelihood estimation (MLE) is used for estimating the parameters of the linear model

175   along with the fitting error (assumed to be normally distributed and un-biased). From the MLE method, the standard deviations and correlations of the estimated parameters (Sørensen, 2011) are obtained. The linear model is expressed by means of the following Eq. (5):

$$q_c = X_a\, z + X_b + \varepsilon \,, \tag{5}$$

where X_a, X_b are stochastic variables modelling parameter uncertainty related to the parameters a and b respectively and ε is

180   the fitting error while z is the depth in meters. Table 2 shows a summary of the fitting parameters.

The residuals are then plotted to check the assumption of the normality of model error. For the first layer (Figure 5.a), the distribution of the residual is slightly skewed to the right. This means that the trend line underrepresents the tip resistance due to the presence of high peeks at the boundary layer. For the second layer (Figure 5.b), a normal distribution about the 0 mean is visible, implying that a better fit is achieved.

185

Parameter	Distribution	Mean	Standard Deviation
X_a (1st layer)	Normal	-0.42	0.049
X_a (2st layer)	Normal	-0.53	0.024
X_b (1st layer)	Normal	6.35	0.28
X_b (2st layer)	Normal	34.05	0.72
ε (1st layer)	Normal	0	3.14
ε (2st layer)	Normal	0	16.06 [MPa]
ρ_{X_a,X_b} (1st layer)	-	0.86	-
ρ_{X_a,X_b} (2st layer)	-	0.98	-

Table 2: Stochastic input variable for tip resistance.
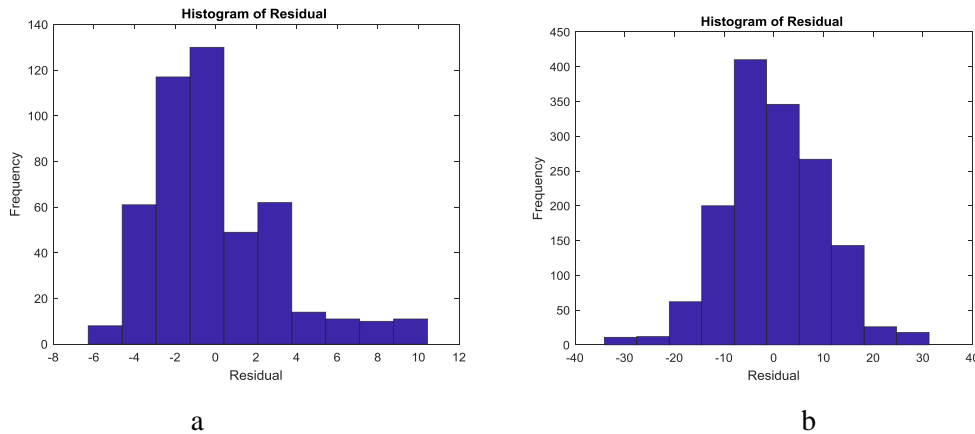
Figure 5: Histogram of residual for layer 1 (a) and layer 2 (b).

The empirical linear relationship is used to calculate the drained constrain modulus in unloading/reloading E_s (Lunne et al.,
190 1997, Lunne and Christoffersen, 1983):

$$E_s = X_\alpha \ q_c \ , \tag{6}$$

where X_α is a unit-less stochastic variable. For over-consolidated sand, typical of offshore conditions, is recommended to
use the value of $\alpha = 5$ (Lunne and Christoffersen, 1983). However there is no unique relation between the stiffness modulus
and the tip resistance because the α value is highly dependent on the soil, stress history, relative density, effective stress level
195 and other factors (Lunne et al., 1997, Bellotti et al. 1989, Jamiolkowski et al. 1988).

In order to understand the uncertainty in the stiffness modulus, α is treated as stochastic normal variable varying from $\alpha_{min} = 3$ to $\alpha_{max} = 8$ with a mean μ=5.5 and standard deviation σ=1.25. The standard deviation is calculated by $(\alpha_{min} - \alpha_{max})/4$ assuming that 95.4 % of the values are enclosed between the α values of 3 and 8.

Thus calculation of the drained constrain modulus in unloading/reloading covering all possible uncertainties is summarized
200   as follows:

$$E_s = \boldsymbol{X}_\alpha \left[\boldsymbol{X}_a \, z + \boldsymbol{X}_b + \varepsilon \right], \tag{7}$$

Depending on the size of the foundation, the local fluctuation (physical uncertainty) of the tip resistance can have a significant impact on structural behaviour. If the size of the foundation is large enough, the soil behaviour is governed by the average of the global variability of the tip resistance (mean trend value). For a smaller foundation, the local effect, i.e. the
205   local physical variability of the tip resistance, is governing the soil behaviour. If the local variability of the tip resistance is not affecting the foundation behaviour compared to the fitted linear model, it can be neglected. Moreover, the uncertainty related to the empirical formulation for calculating the soil stiffness ($\boldsymbol{X}_\alpha$), has a higher influence compared to the one used to approximate the tip resistance with a linear model ($\boldsymbol{X}_a, \boldsymbol{X}_b, \varepsilon$). Preliminary results show that the uncertainty associated with approximating the tip resistance with the mean trend line is negligible due to the size of the monopile. For this reason
210    $\boldsymbol{X}_a, \boldsymbol{X}_b, \varepsilon$ are considered deterministic at their mean value.

Figure 6 shows the variability of the soil modulus E_s over depth. The red lines are the realizations, using MC simulation by performing random sampling on the stochastic variable $\boldsymbol{X}_\alpha$. The black points are the deterministic multiplication of the tip resistance with the mean value of $\alpha = 5.5$.
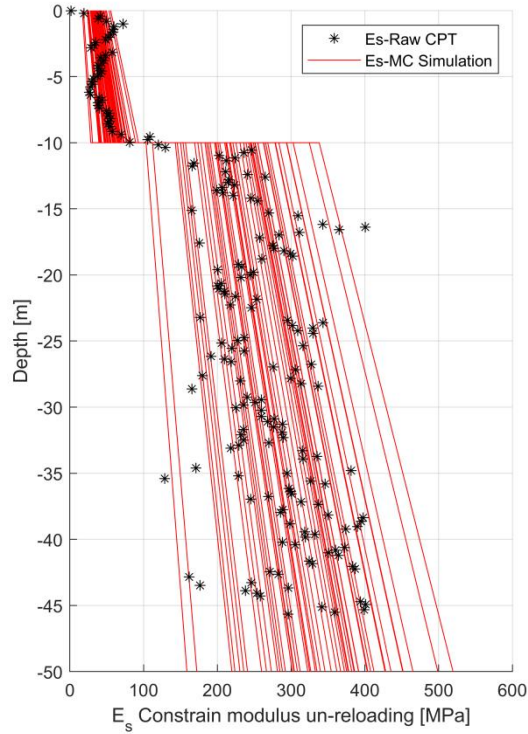
215
Figure 6: Variability of the soil modulus E_s over depth.

The drained constrain modulus in unloading/reloading E_s is then converted to the drained triaxial Young's modulo in unloading/reloading E_{ur} used in the Mohr-Coulomb soil model in PLAXIS. Assuming an elastic behaviour of the soil during unloading/reloading, E_s and E_{ur} can be related by means of:

$$E_{ur} = \frac{(1-v_{ur})}{(1+v_{ur})*(1-2*v_{ur})} E_s ,$$ (8)

220   where v_{ur} is the Poisson ratio of 0.2

In reality the soil stiffness depends on depth. In the Mohr-Coulomb model a linear increase of stiffness with depth is accounted for using the following formula:

$$E(z)_{ur} = E(z)_{ur}^{ref} + (z_{ref} - z) E_{inc} ,$$ (9)

where $E(z)_{ur}$ is the Young's modulo for unloading/reloading at a depth z, $E(z)_{ur}^{ref}$ is the Young's modulo for

225   unloading/reloading at a reference depth z_{ref} and E_{inc} is the increment of the Young's modulo. Using this equation for a

given input value of E_{ur}^{ref} and the increment E_{inc}, the E_{ur} can be derived at the specific depth below surface and compared to

E_s, as specified in the design soil profile. For all realizations of the different soil stiffnesses (Figure 6 red lines), E_{ur}^{ref} and the increment E_{inc} are calculated:

- For the first layer at $z_{ref} = 0$: $\mu_{E_{ur}^{ref}} = 32.25\ MPa$ and $\sigma_{E_{ur}^{ref}} = 7.06\ MPa$

230

- For the second layer at $z_{ref} = -10\ m$: $\mu_{E_{ur}^{ref}} = 196.90\ MPa$ and $\sigma_{E_{ur}^{ref}} = 43.14\ MPa$

Other soil properties such as the specific weight, friction angle and relative density are considered to be deterministic. A full positive correlation between the two soil layer stiffness is assumed.

3.2.2 Cyclic contour diagrams

The aim of the contour diagrams is to provide a 3D variation of the accumulated permanent strain in function of the Average

235 Stress Ratio (ASR, average shear stress divided by the initial vertical pressure or confining pressure), Cyclic Stress Ratio (CSR, cyclic shear stress divided by the initial vertical pressure or confining pressure) and the number of cycles (N). An extensive laboratory test campaign is needed in order to have an accurate 3D contour diagram. The laboratory campaign generally consists of carrying out different regular cyclic load tests with different average and cyclic amplitude stresses for a certain number of cycles.

240 For this work a series of undrained single-stage two-way cyclic simple shear tests have been performed at the Soil Mechanics Laboratories of the Technical University of Berlin. The tests were carried out on reconstituted soil sample. The samples were prepared by means of air pluviation method. The initial vertical pressure was 200 kPa and no pre-shearing was considered.

The cyclic behaviour of the upper layer sand was evaluated with samples prepared at a relative density of 70%. For the lower

245 layer sand, a 90% relative density was used. Two-way cyclic loading tests were carried out, testing different combinations of ASR and CSR. All tests were stopped at 1000 cycles or at the start of the cyclic mobility phase. For the results on cyclic behaviour of the different tests and relative densities, reference is made to Zorzi et al. (Zorzi et al., 2019.b).

All data extracted from the laboratory tests were assembled in a three-dimensional matrix (ASR, CSR, N) and a three-dimensional interpolation of the permanent shear strain (γ_p) was created to map the entire 3D space. The repeatability of

250 cyclic simple shear tests is an important aspect to consider in evaluating the uncertainties in the cyclic contour diagram. Cyclic simple shear tests feature a low repeatability for dense sand which can be attributed to the relatively small specimen size used for testing (Vanden Bergen, 2001). This makes the cyclic tests sensitive to sample preparation such as different initially measured relative density, soil fabric and void ratio non-uniformity.

Due to this variability of the test, a mathematical formulation was fitted to the raw interpolation. For this reason, different

255 two-dimensional slices (CSR vs N) at different ASR were extracted. Figure 7 represents one slice for ASR equal to 0.06. The different coloured points represent the strain surfaces γ_p for different levels of deformation. The raw interpolation of data and the uncertainty related to low sample repeatability of the tests cause an unrealistic non-smooth shape of the strain surfaces.

Therefore, each slice is assumed to follow a power law function (variation of CSR as power of N) for different strain levels and then calibrated to fit the data. Finally, the calibrated strain surfaces are interpolated to create the final smooth 3D contour

260   diagram. This procedure and its validation are explained in Zorzi et al. (Zorzi et al., 2019a).
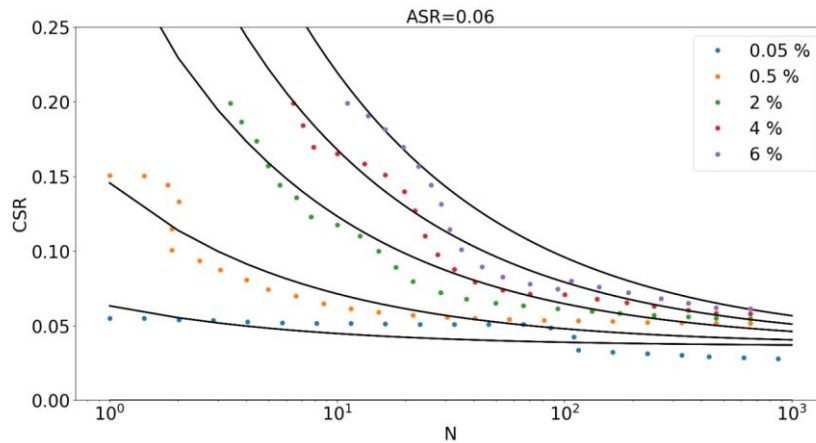
Figure 7: Slice of the cyclic contour diagram.

The power law function in the form of Equation (1).

$$CSR = \mathbf{X}_c \, N^{X_d} + \boldsymbol{X}_e + \varepsilon \,, \tag{10}$$

265   The parameter $\boldsymbol{X}_d$ represents the shape of the curve, $\mathbf{X}_c$ is a scaling factor, $\boldsymbol{X}_e$ is the intersection with the CSR axis and ε is the fitting error. Using the MLM technique it is possible to fit the mathematical model and estimate the standard deviation of the fitting error and the standard deviation of the parameters c and e. During the fitting procedure, the shape parameter d is assumed fixed equal to -0.35 for the lower layer and -0.50 for the upper layer.

Based on the results of the fitting procedure, a standard deviation of the fitting error of 0.008 is chosen for the two diagrams

270   for the two soils. The values c and e are considered deterministic as the standard deviation associated is very low. Preliminary simulations show that the uncertainty of a and c derived from the MLM has less influence than the uncertainty in the fitting error.

It has to be noted that the fitting error is to some extent reflecting the uncertainties of repeatability of the tests. Moreover, the relative density of the soil samples is based on the empirical relation applied to the tip resistance (chapter 3.1). In order to

275   account for the uncertainty in the relative density, different sets of contour diagrams should have been derived from several tests performed with soil samples at different relative densities.

The contour diagrams for two different ASR slices are presented in Figure 8 and Figure 9 for the upper and lower layer, respectively.
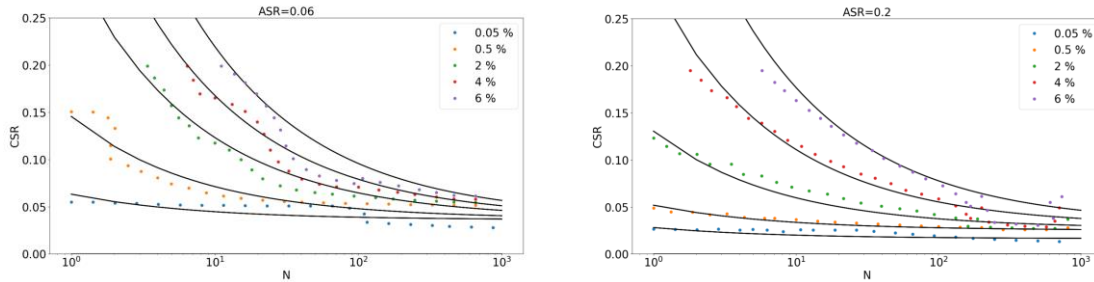
Figure 8: Cyclic contour diagram for the first layer.
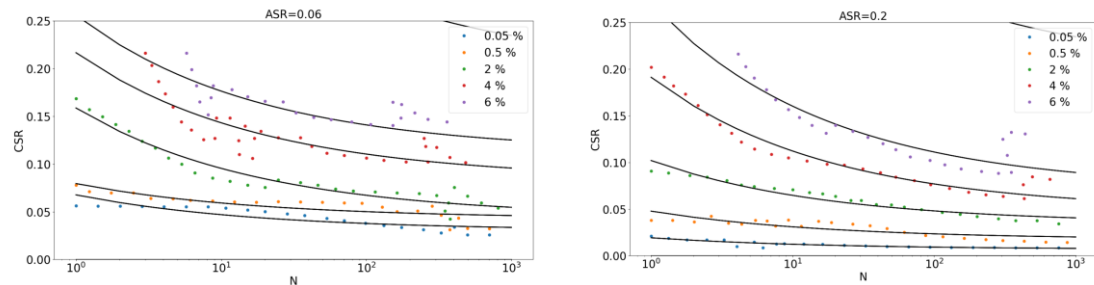
Figure 9: Cyclic contour diagram for the second layer.

3.2.3 Load uncertainty

The load input parameter for the SCD model is characterized by a regular loading package with a mean and cyclic amplitude load and an equivalent number of cycles (hereafter, they are called "load inputs" for simplicity). In common practice the structural engineer provides the irregular history at mudline level by means of the aero-hydro-servo-elastic model. Therefore, a procedure is needed to transform the irregular design storm event to one single regular loading parcel. The environmental load used for the cyclic loading design relies on the chosen return period for the load. The statistical distribution of the environmental loads is then based on different return periods.

The design storm event is here defined as a six hour duration of the extreme load (also called peak of the storm) (DNV-GL, 2017). The underlying assumption in considering only the peak is that most of the deformations which the soil experiences happen at the peak of the storm. The considered design load case is DLC 6.1 (IEC, 2009; BSH, 2015), i.e. when the wind turbine is parked and yaw out of the wind. ULS loads are considered for the cyclic load design.

In order to derive the irregular load history at mudline level, the fully coupled aero-hydro-servo-elastic model is developed in the wind turbine simulation tool, HAWC2. Based on 5-year in-situ metocean data from the North Sea, the environmental contours for different return periods are derived as shown in Figure 10 (Velarde et al, 2019a). The marginal extreme wind distribution is derived using the peak-over-threshold method for wind speed above 25 m/s. Furthermore, it is assumed that maximum responses are given by the maximum mean wind speed and conditional wave height for each return period (red point in Figure 10) [20].
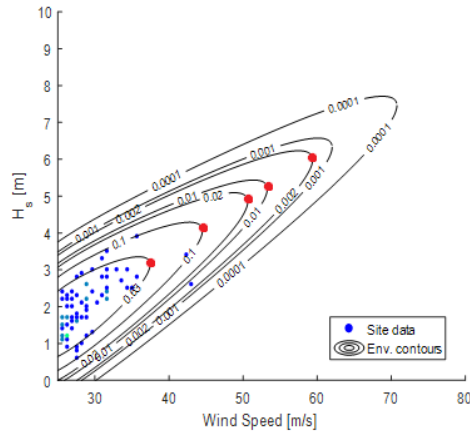
300

Figure 10: Environmental contour plot for extreme sea states (Velarde et al, 2019a).

The 5 design sea states for maximum wind speed are summarized in Table 3. In order to account for short-term variability in the response, 16 independent realizations are considered for each design sea state.

Annual Exceedance Probability (q)	Return period [year]	Wind speed Uw [m/s]	Wave height Hs [m]	Wave period Tp [s]
0.63	1	37.4	3.17	7.95
0.10	10	44.5	4.10	8.84
0.02	50	50.6	4.90	9.54
0.01	100	53.3	5.24	9.83
0.002	500	59.4	6.04	10.44

Table 3: Design sea state for maximum wind speed.

305 Time-domain simulations provide an irregular force history of 10 minutes at the mudline. In order to transform the 10 minute irregular loading to a 6 hr storm, each 10 minutes is repeated 36 times.

The irregular load histories have to be simplified to one equivalent regular package with a specific mean and cyclic load amplitude and an equivalent number of cycles that lead to the same damage accumulation (accumulation of soil deformation) as that of the irregular load series.

310 The following procedure is used (Andersen, 2015):

- The rainflow counting method is utilized to break down the irregular history into a set of regular packages with different combination of mean force F_a and cyclic amplitude force F_{cly} and number of cycles N. Figure 11 shows an example of the output from the rainflow counting.

315
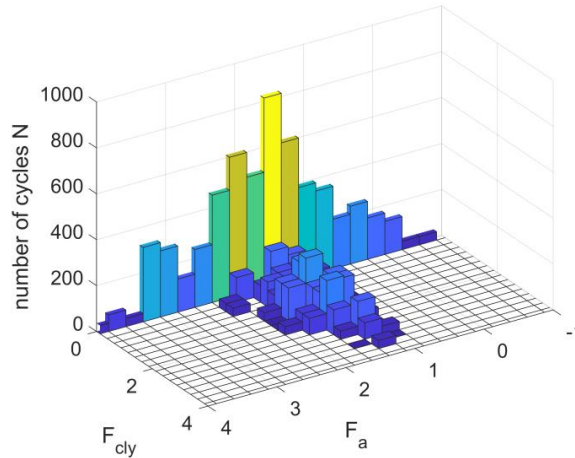
Figure 11: Rainflow matrix for 100 year return period wind speed.

- All the bins are ordered with increasing maximum force F_{max} obtained from the sum of the mean and the cyclic amplitude ($F_{max} = F_a + F_{cly}$).

- 3D contour diagrams in conjunction with the strain accumulation method [21, 2] are then used to calculate the accumulation of deformation. After scaling the loads to shear stresses, the result of this procedure gives the

320   equivalent number of cycles for the highest maximum force F_{max}^{max}, which in turn gives the same accumulation of deformation of the irregular load history.

This procedure is applied for all simulations of the different return periods.

To obtain the statistical distribution, the mean force, cyclic amplitude force and the equivalent number of cycles are plotted versus the probability of non-exceedance for each return period.

325   The black points in the 3 following figures, are, respectively, the mean load, cyclic amplitude and number of cycles of the regular packages obtained from the previous procedure and plotted vs the probability of not exceedance for each return period. Assuming that for each return period the black points have a normal distribution, the 0.50 fractile (red circles) and the 0.95 fractile (blue circles) are obtained.

The statistical distributions for the loads are derived by fitting a Gumbel distribution to the 0.95 fractile values (NORSOK,

330   2007). The MLM is employed to fit the cumulative Gumbel distribution to the extreme response (blue circles). The cumulative density function distribution is defined as:

$$CDF(x) = \exp(- \exp(-(x - \alpha)/\beta)) , \qquad (11)$$

$$\mu = \alpha + \beta\, 0.5772 , \qquad (12)$$

$$\sigma = \frac{\pi}{2.44}\, \beta , \qquad (13)$$

335 The Table 4 summarizes the parameters of distribution for three load inputs. The standard deviation of the fitting error is small, marking a good fitting of the distribution function.

Load	α	β	μ	σ	σ_ε
F_a	1.092	0,113	1.158 [MN]	0.382 [MN]	0.0040
F_{cly}	3.66	0.093	3.71 [MN]	0.347 [MN]	0.011
N_{eq}	329.75	70.08	370.2 [Cycles]	9.49 [Cycles]	0.024

Table 4: Gumbel parameters of the distribution for the load inputs.

Looking at the distribution of Figure 12 a-b-c, larger 0.50 fractiles (red circles) are present when increasing the return period. This is more pronounced for the mean force and is expected because the higher the return period is, the higher is the mean

340 pressure on the wind turbine tower.
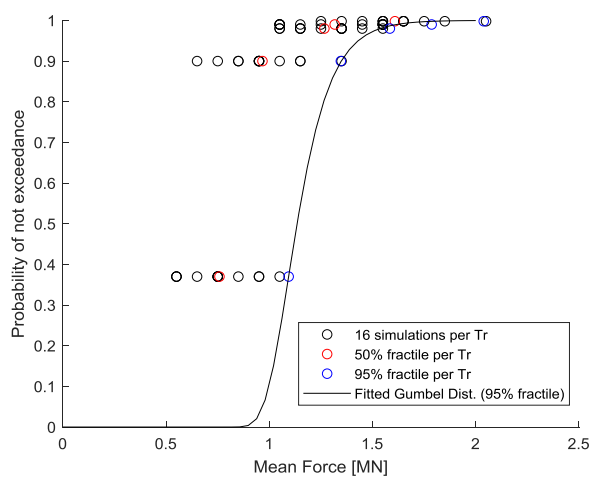
(a)
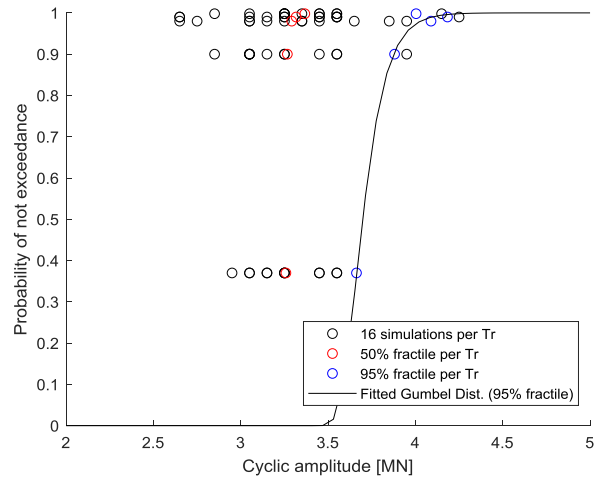
(b)
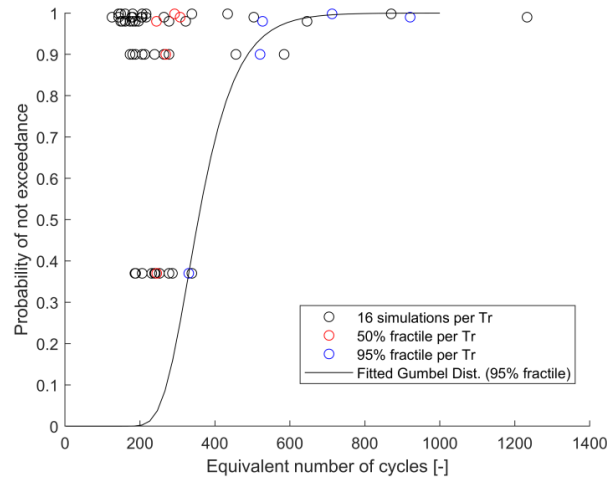
(c)

Figure 12: Distribution of the load inputs.

The scatter for each return period is more significant when the return period is increasing. This can have different reasons: the "rare" storms with a lower probability of occurrence could give more non-linearity problems varying the wave and wind
350 seeds in the aero-hydro-servo-elastic model. It could also depend on the model uncertainty in the time domain simulations. The correlation coefficients ρ for the 0.95 fractile values between the mean and cyclic loads and the equivalent number of cycles are: $\rho_{F_a - F_{cly}} = 0.77$, $\rho_{N_{eq} - F_{cly}} = 0.81$ and $\rho_{N_{eq} - F_a} = 0.85$. The three coefficients mark a strong positive correlation between the three load inputs.

3.2.4 Model error

355   This type of error is difficult to estimate because it requires the validation of the numerical error against different model tests. In the case of the SCD model, this error is arising due to the simplification of the model for a much more complex behaviour of the soil-structure-interaction under cyclic loading. The model error ε_{model} is estimated as a random variable and multiplied to predict the structural tilting (Eq. 14). The model error is assumed to be normally distributed with unitary mean and a coefficient of variation of 10%. Ideally, this model uncertainty should be quantified comparing the results from

360   the SCD model with several different test results. However, such a amount of tests is not feasible.

$$g(\boldsymbol{X}) = \theta_{max} - \varepsilon_{model}\,\theta_{calc}(\boldsymbol{X}) \,, \tag{14}$$

3.3 Derivation of the response surface

The stochastic variables are summarized in Table 5. For simplicity, a full correlation between the soil stiffness of the two layers and the loads is assumed.

X	Unit	PDF	μ	σ	CoV [%]	ρ
Soil stiffness Layer 1 E_{ur}^{ref}	MPa	Normal	32.25	7.06	21.9	
Soil stiffness Layer 2 E_{ur}^{ref}	MPa	Normal	196.90	43.14	21.9	1
Cyclic contour diagrams fitting error CCD_{err}	-	Normal	0	0.008	-	-
Input load F_a	MN	Gumbel	1.158	0.382	32.9	
Input load F_{cly}	MN	Gumbel	3.71	0.347	9.3	1
Input load N_{eq}	Cycles	Gumbel	370.2	9.49	2.5	

365   **Table 5: Summary of the stochastic variables.**

Once the stochastic variables are defined, the 3D FEM model has to be substituted by a response surface. The DoE is used to obtain the training point from FE simulation. As most of the variables are correlated, three stochastic variables are considered: the stiffness of the upper soil layer E_{ur}, the fitting error of the cyclic contour diagram CCD_{err} and the mean load F_a. The independent input stochastic variables have the statistical distribution shown in Tab 5. For each factor, three different

370   levels are assumed: minimum value $\mu - 2 * \sigma$, average value μ and maximum value $\mu + 2 * \sigma$. A full factorial design in three levels is implemented. Therefore, 33 simulations are needed to explore all possible combination.

A second-order polynomial function is fitted to the sample data. The linear regression method is used to estimate regression coefficients of the polynomial function. The following function is the outcome of the linear regression analysis:

$$\theta_{calc} = 0.248\, F_a - 0.007\, E_{ur}\, F_a - 0.144\, F_a\, CCD_{err} + 0.0000746\, E_{ur}{}^2\, F_a + \varepsilon_{fit} \, , \tag{15}$$

375 An un-biased fitting error (ε) with normal distribution is assumed and the estimate of residual standard deviation ($\sigma_{\varepsilon_{fit}}$) is 0.0013. R-squared is a statistical measure of how close the data is to the fitted regression line. For the fitted function, the R-squared value is 0.9984 underlining a good fit of the function to the data.

Figure 13.a shows the function at the $CCD_{err} = 0$ (the mean value). The surface shows that at a lower soil stiffness and a high force, a higher rotation of the monopile is reached. Values higher than 0.25 are considered as failure. The red points are

380 the numerical simulations. The 3D plot (Figure 13.b) shows the response surface for the mean value of the force $F_a =$ 1.158 MN. It is apparent that the fitting error for the contour diagram is small and thus does not have a significant influence on the results.

a)   b)
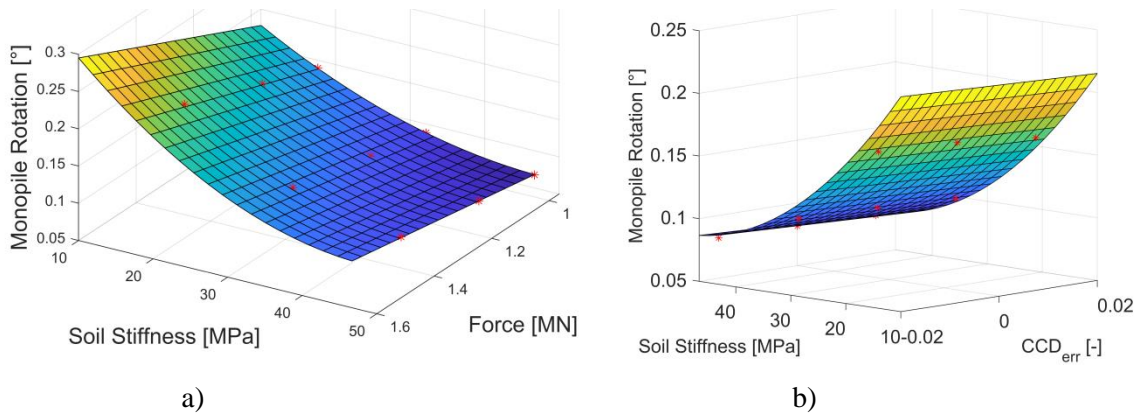
385 **Figure 13: Response surfaces.**

3.4 Reliability analysis

The limit state function is written as:

$$g(\boldsymbol{X}) = 0.25° - (0.248\, F_a - 0.007\, E_{ur}\, F_a - 0.144\, F_a\, CCD_{err} + 0.0000746\, E_{ur}{}^2\, F_a + \varepsilon_{fit})\, \varepsilon_{model} \, , \tag{16}$$

10^7 MC simulations are performed by random sampling of the input stochastic variables. This number is the minimum

390 number to keep the relative error of the reliability index lower than 1%. With the analysed monopile design, the annual probability of failure is 2.7000e-05 and the corresponding annual reliability index is 4.03. This means, that the monopile meets the target reliability index of 2.9-3.3 and is considered safe in long-term behaviour in terms of rotation accumulation for the design storm event.

3.5 Sensitivity analysis

395 The sensitivity analysis of the stochastic input variables on the reliability index is conducted by varying the coefficient of variation one at a time for each input (0.5 CoV and 2 CoV). The inclination of dashed lines in Figure 14 marks the sensitivity of the stochastic variable. Mean force F_a and the soil stiffness E_{ur} are both influencing the reliability index significantly more than the fitting error and numerical model error do.
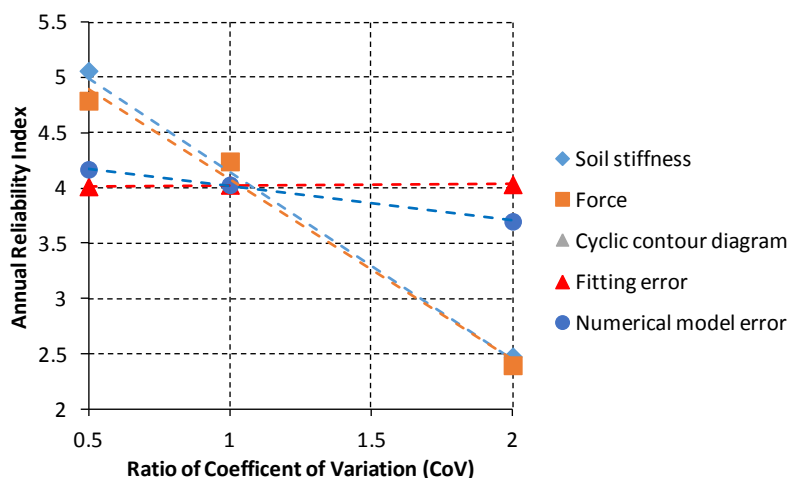
400   **Figure 14: Sensitivity plot.**

4. Conclusion

During the lifetime of wind turbines, storms, typhoons or seismic action are likely to cause permanent rotation of the structure due to the accumulation of plastic strain in the soil surrounding the foundation. The serviceability limit state criteria requires that the long-term structural tilting does not exceed the operational tolerance prescribed by the wind turbine

405 manufacturer (usually less than 1°) with a specific target reliability level. In this paper, the SLS design for long-term structural tilting is addressed within a reliability framework. This framework is developed based on 3D FE models for the prediction of the SSI under cyclic loading. For the case study of a large monopile installed on a typical North Sea environment, a reliability index of 4.03 is obtained. Sensitivity analysis also shows that uncertainties related to soil stiffness and environmental loads significantly affect the reliability of the structure. For regions where assessment against accidental

410 loads due to typhoons are necessary, uncertainty of the extreme environmental loads can increase by up to 80%. Such load scenarios can significantly reduce the reliability index, and therefore become the governing limit state.

A discussion has to be started in the offshore community regarding the very strict tilting requirement (i.e., 0.25°). This very small operational restriction can lead to foundations of excessive dimensions which are unfeasible from an economic point of view. On the other hand, a less strict verticality requirement (which could be a function of the dimension and type of the

415 installed wind turbine), for example an angle of rotation of 1-3°, can lead to a smaller foundation size and still be meeting

safety requirements. For this reason, other checks for the basis for the aero-elastic analyses, the position of the natural frequency of the whole system and fatigue analysis when a wind turbine is tilted at 1-3°, have to be carried out to ensure achievement of the planned lifetime. Allowing a less stringent tilting of the foundation can also be beneficial during the monopile installation. A small foundation dimension saves vessel and equipment cost, which contributes significantly to the
420   lower final cost of the foundation.

Code and data availability

The codes can be made available by contacting the corresponding author.

Author contribution

Zorzi, Mankar, Velarde and Sørensen designed the proposed methodology. Zorzi prepared the manuscript with the
425   contributions from all co-authors.

Competing interests

The authors declare that they have no conflict of interest.

Acknowledgement

This research is part of the Innovation and Networking for Fatigue and Reliability Analysis of Structures - Training for
430   Assessment of Risk (INFRASTAR) project. This project has received funding from the European Union's Horizon 2020 research and innovation program under the Marie Skłodowska-Curie grant agreement No. 676139. The laboratory tests are provided by the Chair of Soil Mechanics and Geotechnical Engineering of the Technical University of Berlin. The authors are grateful for the kind permission to use those test results.

References

435   Andersen, K.H.: Cyclic soil parameters for offshore foundation design, Frontiers in Offshore Geotechnics III, ISFOG'2015,
        Oslo, Norway, 10-12 June 2015, 5-82, doi: 10.1201/b18442-4, 2015.

Baldi, G., Bellotti, R., Ghionna, V., Jamiolkowski, M., and Pasqualini, E.: Interpretation of CPTs and CPTUs; 2nd part:
        drained penetration of sands, Proc. 4th Int. Geotech. Seminar, Singapore, 143-156, 1986

Bellotti, R., Ghionna, V.N., Jamiolkowski, M., and Robertson, P.K.: Design parameters of cohesionless soils from in situ
440   tests, Transportation Research Record, 1235, 0361-1981, 1989.

Bhattacharya, S.: Challenges in Design of Foundations for Offshore Wind Turbines, Engineering & Technology Reference, 9, doi: 10.1049/etr.2014.0041, 2014.

Bhattacharya, S.: Design of foundations for offshore wind turbines, Wiley, doi: 10.1002/9781119128137, 2018.

BSH: Standard Design - minimum requirements concerning the constructive design of offshore structures within the
445   Exclusive Economic Zone (EEZ), Federal Maritime and Hydrographic Agency (BSH), 2015.

DNV-GL: DNVGL-RP-C212 - Offshore soil mechanics and geotechnical engineering, 2017.

Fenton, G. and Griffiths, D.: Risk assessment in geotechnical engineering, John Wiley & Sons, doi: 10.1002/9780470284704, 2008.

IEC: IEC 61400-3 - Wind turbines Part 3: Design requirements for offshore wind turbines, International Electrotechnical
450   Commission, 2009.

Jamiolkowski, M., Ghionna, V., Lancellotta, R., and Pasqualini, E.: New correlations of penetration tests for design practice, International Journal Of Rock Mechanics And Mining Sciences & Geomechanics, 27(2), A91, doi: 10.1016/0148-9062(90)95078-f, 1990.

Larsen T. J. and Hansen A. M.: How 2 HAWC2, the user's manual, Risø National Laboratory, 2015.

455 Lunne, T. and Christoffersen, H. P.: Interpretation of Cone Penetrometer Data for Offshore Sands, Offshore Technology Conference, Houston, Texas, 2-5 May 1983, doi:10.4043/4464-MS, 1983.

Lunne, T., Robertson, P.K. and Powell, J.J.M.: Cone Penetration Testing in Geotechnical Practice, CRC Press, London, doi: https://doi.org/10.1201/9781482295047, 1997.

NORSOK : NORSOK Standard N-003, Actions and action effects, 2007.

460 PLAXIS :. Plaxis 3D Reference Manual, Edited by Brinkgreve, R.B.J., Kumarswamy, S., Swolfs, W.M., and Foria F., 2017.

Sørensen J. D.: Notes in Structural Reliability Theory and Risk Analysis, Aalborg University, 2011.

Vanden Bergen J.F.: Sand Strength Degradation within the Framework of Vibratory Pile Driving, PhD thesis, University Catholique de Louvain, Faculty of Applied Science Civil and Environmental Engineering Division, 2001.

Velarde J., Kramhøft C. and Sørensen JD.: Reliability-based Design Optimization of Offshore Wind Turbine Concrete
465   Structures, 13th International Conference on Applications of Statistics and Probability in Civil Engineering, Seoul, Korea, 26-30 May 2019, doi: https://doi.org/10.22725/ICASP13.185, 2019a.

Velarde, J., Sørensen, J. D., Kramhøft, C., and Zorzi, G.: Fatigue reliability of large monopiles for offshore wind turbines, Submitted to International Journal of Fatigue, 2019b.

Wu, T., Tang, W., Sangrey, D., and Baecher, G.: Reliability of Offshore Foundations-State of the Art, Journal of
470   Geotechnical Engineering, 115, 157-178. doi: 10.1061/(asce)0733-9410(1989)115:2(157), 1989.

Zorzi, G., Richter, T., Kirsch, F., Augustesen, A. H., Østergaard, M. U., and Sørensen, S. P.: Explicit Method to Account for Cyclic Degradation of Offshore Wind Turbine Foundations Using Cyclic Inter-action Diagrams, International Society of Offshore and Polar Engineers, Sapporo, Japan, 10-15 June 2018, ISOPE-I-18-271, 2018.

Zorzi, G., Kirsch, F., Richter, T., Østergaard, M., and Sørensen, S.: Validation of explicit method to predict accumulation of
475   strain during single and multistage cyclic loading, Proceedings of the XVII ECSMGE-2019 - Geotechnical Engineering
foundation of the future, Reykjavik, Iceland, 1-6 September 2019, 2019a.

Zorzi, G., Kirsch, F., Richter, T., Østergaard, M., and Sørensen, S.: Comparison of cyclic simple shear tests for different
types of sands, 2nd International Conference on Natural Hazards & Infrastructure, Chania, Greece, 23-26 June 2019,
2019b.